Pulsed-laser evaporation technique for deposition of thin films: Physics and theoretical model

Rajiv K. Singh and J. Narayan
Department of Material Science and Engineering, North Carolina State University, Raleigh, North Carolina 27695-7916
(Received 20 June 1989; revised manuscript received 9 January 1990)

We have studied in detail the physical phenomena involved in the interaction of high-powered nanosecond excimer-laser pulses with bulk targets resulting in evaporation, plasma formation, and subsequent deposition of thin films. A theoretical model for simulating these laser-plasma–solid interactions has been developed. In this model, the laser-generated plasma is treated as an ideal gas at high pressure and temperature, which is initially confined in small dimensions, and is suddenly allowed to expand in vacuum. The three-dimensional expansion of this plasma gives rise to the characteristic spatial thickness and compositional variations observed in laser-deposited thin films of multicomponent systems. The forward-directed nature of the laser evaporation process has been found to result from anisotropic expansion velocities of the atomic species which are controlled by the dimensions of the expanding plasma. Based on the nature of interaction of the laser beam with the target and the evaporated material, the pulsed-laser evaporation (PLE) process can be classified into three separate regimes: (i) interaction of the laser beam with the bulk target, (ii) plasma formation, heating, and initial three-dimensional isothermal expansion, and (iii) adiabatic expansion and deposition of thin films. The first two processes occur during the time interval of the laser pulse, while the last process initiates after the laser pulse terminates. Under PLE conditions, the evaporation of the target is assumed to be thermal in nature, while the plasma expansion dynamics is nonthermal as a result of interaction of the laser beam with the evaporated material. The equations of compressible gas dynamics are set up to simulate the expansion of the plasma in the last two regimes. The solution of the gas-dynamics equations shows that the expansion velocities of the plasma are related to its initial dimensions and temperature, and the atomic weight of the species. Detailed simulations analyzing the salient features of the laser-deposition process have been carried out. The effects of various beam and substrate parameters including pulse energy density, substrate-target distance, irradiated spot size, and atomic mass of the species have been theoretically analyzed. This model predicts most of the characteristic experimental features of the laser evaporation and deposition of thin films. These characteristic features include (a) the effect of pulse energy density on atomic velocities, (b) the forward-directed nature of the deposit and its dependence on energy density, (c) spatial compositional variations in multicomponent thin films as a function of energy density, (d) dependence of the atomic velocities with atomic weights of various species in multicomponent films, (e) athermal non-Maxwellian-type velocity distribution of the atomic and molecular species, and (f) thickness and compositional variations as a function of substrate-target distance and irradiated spot size.

I. INTRODUCTION

Lasers have been used in the last three decades to produce high-temperature and high-density plasmas for fusion devices by vaporizing a small amount of material with high-powered nanosecond pulses. Temperatures as high as 10^5–10^7 K have been achieved by this method. Recently, excimer lasers at lower power densities have been used to deposit semiconducting and high-T_c superconducting thin films from bulk targets.[1–8] The deposition characteristics of the pulsed-laser evaporation (PLE) technique for formation of thin films have been found to be significantly different from other vaporization methods. The luminous high-temperature plasma formed in the laser evaporation of targets elongates preferentially perpendicular to the surface.[9,10] The kinetic energies of the ejected species are in the range of 10–100 eV for excimer-laser-irradiated Y-Ba-Cu-O targets, whereas the thermal evaporation energies are approximately an order of magnitude lower.[11] The velocity distribution of PLE species is much broader than an ideal Maxwellian distribution.[12–14] These characteristics of laser-generated plasma have been attributed to the high evaporation flux rates and the interaction of the laser irradiation with the evaporated material. The plasma particle density is in the range of 10^{19}–10^{21} cm^{-3}, depending upon the stage of the expansion process. Other characteristic features of the technique affecting the deposition process have been discussed in detail elsewhere.[15] The laser-deposition process is always forward directed in nature,[16] i.e., most of the evaporated material is deposited preferentially perpendicular to the target spot. Depending on the pulse energy density and other parameters, thickness variations across the film show approximately a $(\cos\theta)^{8-12}$ relationship, where θ corresponds to the angle between the radial vector and target normal.[17] This thickness variation is

much steeper than a $\cos\theta$ variation expected from a conventional thermal evaporation process. Slight spatial compositional variations across multielemental films have been observed, the variation dependent on the pulse energy density.[15] The velocity PLE species have been found to vary as a function of their mass, although their dependence on the mass M is weaker than $M^{-0.5}$ exhibited by thermal evaporation processes.[11,18]

In this paper, we have developed a theoretical model to understand the physics of the laser-solid interaction phenomena, and simulate the nature of the PLE process. This model is based upon the generation of a high-temperature and high-pressure (HT-HP) gaseous plasma which is initially confined to small dimensions and is then suddenly allowed to expand in vacuum. Gas-dynamical equations are set up to simulate the expansion velocities of the plasma. The anisotropic expansion velocities determine compositional and spatial thickness variations in the films. This model shows in detail the effect of various beam and substrate parameters including pulse energy density, substrate-target distance, etc., on the deposition characteristics of PLE.[10] These calculations are compared with our experimental results[15] and other published data.[11] Most of the calculated and experimental results presented are on excimer-laser-irradiated $YBa_2Cu_3O_7$ (1:2:3) superconductors, although the calculations can be easily extended to laser irradiation of other targets.

II. THEORY

To investigate the physics and theoretical nature of the laser-deposition process, the evaporation of the target material, formation of a high-temperature plasma by absorption of the laser energy by the evaporated material, and the expansion of this plasma resulting in deposition of thin films is considered in detail. Depending on the type of interaction of the laser beam with the target, the PLE process can be classified into three separate regimes: (i) interaction of the laser beam with the target material resulting in evaporation of the surface layers; (ii) interaction of the evaporated material with the incident laser beam resulting in an isothermal plasma formation and expansion, and (iii) anisotropic adiabatic expansion of the plasma leading to the characteristic nature of the laser-deposition process. The first two regimes start with the laser pulse and continue until the laser pulse duration. The last regime starts after the laser pulse terminates. Under PLE deposition conditions, where the pulse energy density is in the range of 1–10 J/cm^2, the target evaporation can be considered to be thermal in nature, while the interaction of the laser beam with the evaporated material gives rise to the athermal characteristics of the species in the plasma. Each of the three regimes is considered separately in detail.

A. Interaction of laser beam with the target

The laser-solid interactions in the PLE technique can be divided into two parts: (i) interaction of the laser beam with the bulk target, and (ii) interaction of the laser beam with the evaporated material from the target material. However, the main part of the theoretical model deals with plasma formation, heating, and deposition of the evaporated species. One of the factors affecting the plasma absorption coefficient is the evaporation rate, which is determined by the the laser-solid interactions of the target.

The removal or sputtering of the material from the target by laser irradiation depends on the coupling of the beam with the solid. Intense heating of the surface layers by high-powered nanosecond laser pulses occurs, resulting in melting and/or evaporation of the surface layers, depending on its energy density. These thermal effects of nanosecond interaction of laser beams with metals and semiconductors have been dealt with extensively in the literature.[19,20] Essentially, it involves the solution of the one-dimensional heat flow equation with appropriate boundary conditions taking into account the phase change in the material. The thermal history (heating rate, melting, evaporation) during pulsed-laser irradiation depends on the laser parameters (pulse energy density E, pulse duration τ, shape, and wavelength), and the temperature-dependent optical (reflectivity, absorption coefficient) and thermophysical (heat capacity, density, thermal conductivity, etc.) properties of the material. The presence of a moving interface as a result of melting or evaporation, and time- and temperature-dependent optical and material properties precludes analytical solutions, and numerical solutions like finite difference methods have to be adopted to accurately compute the evaporation characteristics of the pulsed-laser-irradiated materials. Instead of using detailed computer calculations to understand the thermal characteristics of the pulsed-laser-irradiated technique, simpler calculations based on energy balance considerations can be applied to determine the evaporation characteristics as a function of laser and material parameters.[20]

Using simple energy balance considerations, the amount of material evaporated per pulse is calculated. The energy deposited by the laser beam on the target is equal to the energy needed to vaporize the surface layers plus the conduction losses by the substrate and the absorption losses by the plasma. This is given by the energy threshold $E_{\rm th}$, which represents the minimum energy above which appreciable evaporation is observed. As the plasma and other losses may vary with pulse energy density, $E_{\rm th}$ may vary with energy density. The heat balance equation yields

$$\Delta x_t = (1-R)(E-E_{\rm th})/(\Delta H + C_v \Delta T) , \quad (1)$$

where Δx_t, ΔH, C_v, and ΔT are the evaporated thickness, volume, latent heat, volume heat capacity, and the maximum temperature rise, respectively. This equation is valid for conditions where the thermal diffusion distance $(2D\tau)^{1/2}$ is larger than the absorption length of the laser beam in the target material, $1/\alpha_t$. Here, D refers to the thermal diffusivity, and τ is the pulse duration. This condition is generally satisfied for high photon energy radiation of metallic and small band-gap semiconductor materials. However, when $1/\alpha_t > (2D\tau)^{1/2}$ holds, the

thermal conductivity does not play a major role in the evaporation process, and the evaporated depth will be dependent on the attenuation distance ($1/\alpha_t$) of the laser beam in the target material. This may apply in materials where the thermal diffusivity and absorption coefficient are small, e.g., polymers, insulators, etc., which show a logarithmic dependence of the absorption depth with pulse energy density. In Eq. (1), the energy threshold depends on laser wavelength, pulse duration, plasma losses, and the thermal properties of the material. In excimer-laser irradiation, the energy threshold value varies from 0.3–0.4 J/cm^2 for Y-Ba-Cu-O targets to 3.5–4.0 J/cm^2 for silicon.[19] If the material parameters are independent of pulse energy density, a linear increase in evaporated material thickness as a function of pulse energy density will be observed. However, a nonlinear behavior, especially at high-energy densities, may be observed due to the change in plasma losses and reflectivity of the laser beam.[21] Thus, the evaporation flux is dependent on both laser and material parameters which indirectly play an important role in the determination of the plasma absorption coefficient. It should be noted that besides the thermal nature of the sputtering process, nonthermal sputtering processes have also been observed.[13,22] The nature of sputtering does not affect the physics of the deposition process, so it will not be considered in detail. However, it might also be mentioned that the laser-irradiated target surface may exhibit various topographical features including cones, ridges, etc., which have been discussed elsewhere.[22,23]

B. Interaction of laser beam with evaporated material

The high surface temperature induced by laser irradiation leads to emission of positive ions and electrons from a free surface. The thermionic emission of positive ions and electrons from hot surfaces has been widely recognized in the literature.[24] The flux of ions and electrons as a function of temperature can be predicted by the Richardson and Langmuir-Saha equations, respectively. Both of these equations show an exponential increase in the fraction of ionized species with temperature. Higher ionized fractions than predicted by the Langmuir-Saha equation have been observed in laser-irradiated targets.[13] Different mechanisms may play an important part in the ionization of the laser-generated species. Impact ionization, and other mechanisms, especially photoionization, thermal ionization of photon-activated species, and electronic excitation may affect the concentration of the excited species.

The physical mechanisms involved in the absorption and reflection of the laser energy by the evaporating material were identified in the early experiments as the sources for very high-temperature (~ 1 keV) plasma.[25–35] The material evaporated from the hot target is further heated by the absorption of the laser radiation. Although the laser evaporation for the deposition of thin films occurs at much lower power densities, where plasma temperatures[12,36] are of the order of 10^4 K (Refs. 12 and 37), the heating mechanisms and other physical phenomena are similar to the laser-generated high-temperature plasma. It must be noted that at very low electron densities and high neutral atom densities occurring in slightly ionized vapors, electrons are most likely to absorb photons during free-free transitions in collisions with neutral atoms. The absorption of photons by free-free transitions involving neutral atoms, although much less effective than free-free transitions involving ions, may be the dominant mechanism as a result of high neutral atom concentrations. A small proportion of free electrons results in a marked increase in the absorption coefficient, and electron-ion collisions soon become the dominant heating process.

The primary absorption mechanism for a plasma is the electron-ion collisions, i.e., resistance to induced currents.[24] The absorption primarily occurs by an inverse bremsstrahlung process, which involves the absorption of a photon by a free electron. The absorption coefficient α_p of the plasma can be expressed as

$$\alpha_p = 3.69\times 10^8 (Z^3 n_i^2/T^{0.5}\nu^3)[1-\exp(-h\nu/kT)] , \quad (2)$$

where Z, n_i, and T, are, respectively, the average charge, ion density, and temperature of the plasma, and h, k, and ν are the Planck constant, Boltzmann constant, and frequency of the laser light, respectively. The laser energy is highly absorbed if ($\alpha_p X$) is large, where X is the dimension perpendicular to the target of the expanding plasma. This equation shows that the absorption coefficient of the plasma is proportional to n_i^2. Thus, the plasma absorbs the incident laser radiation only at distances very close to the target where the densities of the charged particles are very high. In this equation, we have assumed that the plasma frequency is smaller than the frequency of the laser wavelength, otherwise, all the radiation would be reflected by the plasma. For excimer-laser wavelengths ($\lambda = 308$ nm), the laser frequency is 9.74×10^{14} sec^{-1}. For the same plasma frequency, the critical electron density corresponds to 1.2×10^{22} per cm^3. The high value of the critical electron density means that the reflection losses by the plasma are insignificant for excimer-laser-generated plasmas.

The term $[1-\exp(-h\nu/kT)]$ represents the losses due to stimulated emission. If we consider the excimer-laser wavelength ($\lambda = 308$ nm), the exponential term becomes unity for $T \ll 40\,000$ K and can be approximated by $h\nu/kT$ for $T \gg 40\,000$ K. This absorption term shows a $T^{-0.5}$ dependence for low temperatures ($T \ll 40\,000$ K for $\lambda = 308$ nm, $T \ll 10\,000$ K for $\lambda = 1.06$ μm) and $T^{-1.5}$ for high temperatures. This dependence is an important factor in estimating the effect of energy density on the deposition characteristics. The maximum temperature induced in the plasma is dependent on the laser power density and the laser frequency. Temperatures in the range of 7000–20 000 K have been estimated in the plasma in the case of excimer-laser evaporation of 1:2:3 targets, although the surface evaporation temperature is much lower.[12,25,36] Thus in the PLE regime, the absorption coefficient should generally exhibit a $T^{-0.5}$ dependence for excimer-laser-irradiated 1:2:3 targets, whereas for CO_2 laser ($\lambda = 10.6$ μm) irradiated targets the temperature dependence of the absorption coefficient should

vary as $T^{-1.5}$. The frequency dependence of the absorption coefficient also changes from ν^2 to ν^3, depending on the value of $h\nu/kT$.

As seen from Eq. (2), the heating of the evaporated material is controlled by the plasma absorption coefficient, which depends on the concentration of the ionized species, plasma temperature, wavelength, pulse duration, etc. The particle density in the plasma in turn depends on the degree of ionization, evaporation rate, and the plasma expansion velocities. Moreover, the absorption coefficient shows different temperature dependences for different energy density regimes. Thus, to theoretically compute the absolute value of the plasma absorption coefficient as a function of pulse energy density is difficult, and an approximate method based on dependence of each of the above-mentioned parameters on temperature and energy density is adopted. This method is discussed in detail in later sections.

Because of the high expansion velocities of the leading plasma edge, the electron and ion densities decrease very rapidly with time, which makes the plasma transparent to the laser beam for larger distances away from the target surface. As the plasma is constantly augmented with evaporated particles at its inner edge adjacent to the target surface, a thin region near the surface is constantly absorbing the laser radiation during the time interval of the laser pulse. Based on these observations, a schematic diagram of the laser interaction with the plasma target is shown in Fig. 1. This diagram shows that during the incidence of the laser pulse four separate regions can be distinguished: (i) unaffected bulk target, (ii) evaporating target surface, (iii) area near the surface absorbing the laser beam, and (iv) rapidly expanding outer edge which is transparent to the laser beam. It is reasonable to assume that during the duration of the laser pulse an isothermal temperature is attained near the target surface. A dynamic equilibrium exists between the plasma absorption coefficient and the rapid transfer of thermal energy into kinetic energy. These two mechanisms control the isothermal temperature of the plasma. At even higher energy densities, when an appreciable amount of energy is absorbed by the plasma, a self-regulating regime may exist near the target surface.[29] The assumption of a self-regulating regime at the surface of the target can be justified in the following manner. If the absorption of laser light by the plasma becomes higher (due to lowering of the temperature), the evaporation of the species from the target becomes less, thus decreasing the density of the ionized species. This consequently increases the absorption of laser energy and the temperature of the plasma. If, on the other hand, the absorption of the laser energy is less, the process is reversed, with similar results. It has been theoretically deduced[29] that the density, temperature, and dimension of the plume adjust in such a manner that the plasma absorbs the same amount of laser radiation to maintain a self-regulating regime. During the isothermal regime, assuming an initial expansion velocity of 10^5-10^6 cm/sec, the perpendicular dimension of the plasma at the end of a 30 nsec laser pulse is of the order of $10^{-3}-10^{-2}$ cm. It is assumed that the power absorbed by the plasma is distributed uniformly over its entire mass. This assumption was found to be valid in the laser-generated plasma, where the thermalization time is significantly less than the plasma expansion time, resulting in the establishment of a uniform temperature in the plasma.[28] Thus, in this regime, the plasma is at an isothermal state, with region C continuously absorbing the laser radiation and expanding isothermally outwards (Fig. 1). This region is constantly augmented with particles evaporated from the target surface.

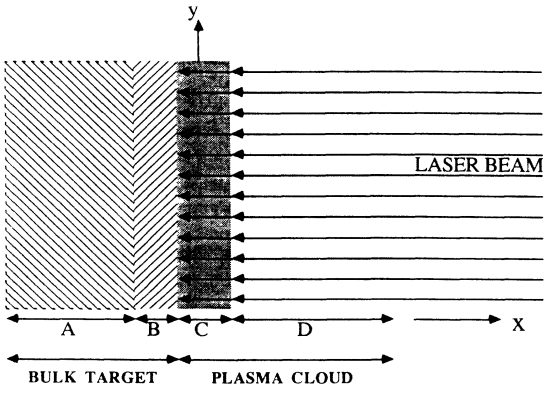

FIG. 1. Schematic diagram showing the different phases present during laser irradiation of a target: (A) unaffected target, (B) evaporated target material, (C) dense plasma absorbing laser radiation, and (D) expanding plasma outer edge transparent to the laser beam.

As the thermal radiative plasma losses show a T^4 temperature dependence, it may be more significant than the target radiative losses. However, calculations[24] have shown that because of the small plasma volume of roughly 10^{-5} cm^3 during the isothermal regime, the radiative losses are insignificant for plasma temperatures below 50–100 eV. Also, the extremely rapid transfer of thermal energy into kinetic energy leads to even smaller radiative losses. It should also be noted that the very short equipartition time for the transfer of energy from the electrons to the ions makes the electron and ion temperatures nearly the same in the PLE regime.

The rapid expansion of the plasma in vacuum results from large density gradients. The plasma which is absorbing the laser energy can be simulated as a HT-HP gas which is initially confined in small dimensions and is suddenly allowed to expand in vacuum. Because of the large pressure gradients initially present near the outer edge (vacuum), very high expansion velocities are induced at this edge. In the initial stages of the plasma expansion when the particle density is of the order of $10^{19}-10^{20}$ cm^{-3}, the mean free path of the particles is short, and the plasma behaves as a continuum fluid. The equations of gas dynamics can be applied to simulate its expansion. In this theoretical formulation, the density and pressure profiles in the plasma are assumed to show an exponential decrease with distance from the target surface. The density (n) of the plasma at any point (x,y,z) at time t can be expressed as a Gaussian function given by

$$n(x,y,z,t)=\frac{N_T t}{2^{0.5}\pi^{1.5}\tau X(t)Y(t)Z(t)} \times\exp\left[-\frac{x^2}{2X(t)^2}-\frac{y^2}{2Y(t)^2}-\frac{z^2}{2Z(t)^2}\right] \quad t\le\tau\ , \tag{3}$$

where N_T is the total number of evaporated particles at the end of the laser pulse ($t=\tau$). $X(t)$, $Y(t)$, and $Z(t)$ are the dimensions of the expanding plasma in the three orthogonal directions, and correspond to the distance at which the plasma density decreases to 60.65% of the inner edge value (maximum density). Since the evaporation rate of the target is constant, a linear increase in the number of particles in the plasma during the time of incidence of the laser pulse is incorporated in the above equation. Fader[31] has deduced that for time scales greater than 4 nsec, a Gaussian density profile in the plasma develops. However, from thermodynamic considerations one expects that the density profile of the plasma species should be dependent on the degree of excitation which affects the specific heat capacity ratio γ. This factor has been considered in detail elsewhere.[38] Since we have assumed that the plasma behaves as an ideal gas, the pressure P at any point in the plasma is related to its density by the ideal gas equation ($P=nkT_0$) and can be expressed as

$$P(x,y,z,t)=\frac{N_T tkT_0}{2^{0.5}\pi^{1.5}\tau X(t)Y(t)Z(t)} \times\exp\left[-\frac{x^2}{2X(t)^2}-\frac{y^2}{2Y(t)^2}-\frac{z^2}{2Z(t)^2}\right] \quad t\le\tau\ , \tag{4}$$

where T_0 is the isothermal temperature of the plasma. Dawson[27] has argued that for maintaining a Gaussian density profile, the velocity should be proportional to distance from the target. A self-similarity expression for the spatial and temporal dependence of the velocity $\mathbf{v}(x,y,z,t)$ can be expressed as

$$\bar{\mathbf{v}}(x,y,z,t)=\frac{x}{X(t)}\frac{dX(t)}{dt}\mathbf{i}+\frac{y}{Y(t)}\frac{dY(t)}{dt}\mathbf{j}+\frac{z}{Z(t)}\frac{dZ(t)}{dt}\mathbf{k} \tag{5}$$

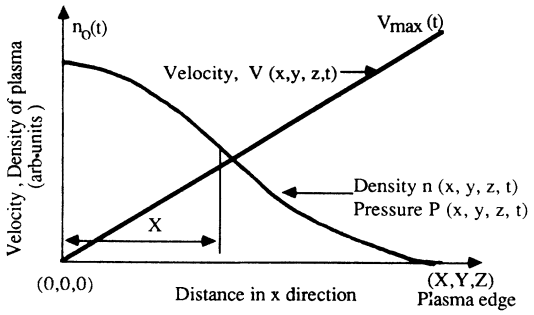

FIG. 2. Schematic profile showing the density (n), pressure (P), and velocity (v) gradients in the plasma in the x direction, which is perpendicular to the target surface. The density and plasma gradients are monotonically decreasing from the target surface with a linear increase in the velocity.

where dX/dt, dY/dt, and dZ/dt refer to the expansion velocities of the plasma edges X, Y, and Z, respectively. The density, pressure, and velocity profiles in the plasma have been shown schematically in Fig. 2. The above expressions show that at the inner edge of the plasma, the density is maximum, while the velocity is minimum.

The equation of gas dynamics governing the expansion of the plasma is the equation of continuity and the equation of motion. The equation of energy is not solved in this regime because we have assumed a constant and uniform temperature within the plasma. As there is an injection of particles in the plasmas in this regime, the equation of continuity can be expressed as

$$-\frac{\partial}{\partial t}\int_v \rho\, dV=\int_S \rho(\bar{\mathbf{v}}\cdot\hat{\mathbf{N}})dA-\frac{\partial}{\partial t}\frac{mN_T t}{\tau}\ , \tag{6}$$

where V denotes the volume, and the surface enclosing V is denoted by S. The differential volume element is denoted by dV, the differential area element by dA, and $\hat{\mathbf{N}}$ is the unit normal vector. In the above equation ρ corresponds to the density of the fluid and m to the mass of the atomic species. This equation simply states the conservation of mass for each atomic species. The last term in Eq. (6) shows the injection of atomic species into the plasma. The equation of the conservation of linear momentum or the equation of motion can be expressed as

$$\int_V\left[\rho\frac{\partial\bar{\mathbf{v}}}{\partial t}+\bar{\mathbf{v}}\frac{\partial\rho}{dt}+\rho(\bar{\mathbf{v}}\cdot\nabla)\bar{\mathbf{v}}+\bar{\mathbf{v}}(\bar{\mathbf{v}}\cdot\nabla P)+\rho\bar{\mathbf{v}}(\nabla\cdot\bar{\mathbf{v}})+\nabla P\right]dV=0\ . \tag{7}$$

If we substitute the relations for the velocity, density, and pressure in Eqs. (6) and (7), we finally arrive at a solution given by the following expression:

$$X(t)\left[\frac{1}{t}\frac{dX}{dt}+\frac{d^2X}{dt^2}\right]=Y(t)\left[\frac{1}{t}\frac{dY}{dt}+\frac{d^2Y}{dt^2}\right]=Z(t)\left[\frac{1}{t}\frac{dZ}{dt}+\frac{d^2Z}{dt^2}\right]=\frac{kT_0}{M}\quad t\le\tau\ . \tag{8}$$

The above equation determines the initial expansion of three orthogonal plasma edges. The initial dimensions of the plasma are of the order of mm in the transverse direction, whereas in the perpendicular direction they are less than 1 μm. As the velocities are controlled by the pressure gradients, the expansion is anisotropic in the direction perpendicular to the target. Equation (8) also shows that in the initial stages of the expansion, when the ex-

pansion velocities are low, the acceleration is very high. Once the expansion velocities increase, the acceleration starts to diminish and ultimately becomes zero, resulting in a similar elongated plasma shape.

C. Adiabatic plasma expansion and deposition of thin films

In the preceding subsection, we examined the plasma formation and its initial isothermal expansion during the incidence of the laser pulse. In the following, we analyze the adiabatic expansion of this plasma in vacuum after the termination of the laser pulse which gives rise to the characteristic nature of the laser-deposition process. After the termination of the laser pulse, no particles are evaporated or injected into the inner edge of the plasma. Also, an adiabatic expansion of the plasma occurs where the temperature can be related to the dimensions of the plasma by the adiabatic thermodynamic equation given by

$$T[X(t)Y(t)Z(t)]^{\gamma-1}=\text{const} ,$$

where γ is the ratio of the specific heat capacities at constant pressure and volume. The thermal energy is rapidly converted into kinetic energy, with plasma attaining extremely high expansion velocities. It has been found for spherical plasmas that the temperature drops off rapidly as the plasma expands; however, the drop is smaller at lower temperatures because energy is regained in the recombination of the ions. The maximum attainable velocity for any gas in vacuum is given by $2a/\gamma-1$, where a is the velocity of sound $[a=(\gamma RT/M)^{0.5}]$. Thus, the maximum attainable velocity or asymptotic velocity is about 3–10 times the velocity of the sound, depending upon the value of γ.

In the adiabatic expansion regime, the velocity of the plasma increases due to a decrease in thermal energy of the plasma. As there is no injection of particles in the inner edge of the plasma, the density and pressure gradients can be expressed in a similar form as shown in Eqs. (3) and (4), by neglecting the term (t/τ) which takes into account the injection of particles into the plasma. The density (n) and the pressure (P) in the plasma can be expressed as

$$n(x,y,z,t)=\frac{N_T}{2^{0.5}\pi^{1.5}X(t)Y(t)Z(t)}\times\exp\left[-\frac{x^2}{2X(t)^2}-\frac{y^2}{2Y(t)^2}-\frac{z^2}{2Z(t)^2}\right] \quad t>\tau , \tag{9}$$

$$P(x,y,z,t)=\frac{N_T kT_0}{2^{0.5}\pi^{1.5}X(t)Y(t)Z(t)}\times\exp\left[-\frac{x^2}{2X(t)^2}-\frac{y^2}{2Y(t)^2}-\frac{z^2}{2Z(t)^2}\right] \quad t>\tau . \tag{10}$$

The velocity expression remains similar to Eq. (5) as in the previous isothermal regime. The equations of the gas dynamics which dictate the expansion of the plasma are the same as in the previous regime except that the equation of energy and adiabatic equation of state also need to be solved. The adiabatic equation of state is given as

$$\frac{1}{P}\left[\frac{\partial P}{\partial t}+\bar{v}\cdot\nabla P\right]-\frac{\gamma}{n}\left[\frac{\partial n}{\partial t}+\bar{v}\cdot\nabla n\right]=0 , \tag{11}$$

and the equation of temperature is given by

$$\frac{\partial T}{\partial t}+\bar{v}\cdot\nabla T=(1-\gamma)T\nabla\cdot\bar{v} . \tag{12}$$

We have assumed that there are no spatial variations in the plasma temperature, or $\nabla T=0$. If we substitute the velocity, density, and the pressure profiles into the differential equations [Eqs. (5), (6), (11), and (12)], the solution which controls the expansion of the plasma in this regime is obtained. This is given by

$$X(t)\left[\frac{d^2X}{dt^2}\right]=Y(t)\left[\frac{d^2Y}{dt^2}\right]=Z(t)\left[\frac{d^2Z}{dt^2}\right]=\frac{kT_0}{M}\left[\frac{X_0Y_0Z_0}{X(t)Y(t)Z(t)}\right]^{\gamma-1} \quad t>\tau , \tag{13}$$

where X_0, Y_0, and Z_0 are the initial orthogonal edges of the plasma after the termination of the laser pulse $(t=\tau)$. The above equation shows that acceleration of the plasma species depends upon the temperature and dimensions of the plasma, and the mass of the species. It should be noted that this hydrodynamic model is based on the equations of fluid flow, and the expansion velocities are controlled by pressure gradients in the plasma. Thus, this model applies to all species including atoms, ions, molecules, neutrals, small clusters, etc. However, based on the difference in their masses, the expansion velocities may be different for different species.

In this regime, the initial transverse dimensions (Y or $Z\sim1$–4 mm) are much larger than the perpendicular dimension ($X\sim20$–100 μm) which correspond to the expansion length in the isothermal regime. As the velocities are dictated by these lengths, the highest velocities are in the direction of the smallest dimension. This gives rise to the characteristic plasma shape elongated outward from the surface. The above equation also shows that if, initially, the plasma is longer in the y than in the z direction, it will be accelerated more rapidly in the z direction. As the plasma expands, most of the thermal energy is converted into kinetic energy, and there is no more energy left for the expansion process. Thus, the plasma becomes elongated in the shorter dimensions and retains its profile during the deposition process. This is shown schematically in Fig. 3(a) and Fig. 3(b), where the plasma initially is elliptical in shape with the y axis being the major axis. After adiabatic expansion, the plasma still retains its elliptical appearance, but in this case the major axis corresponds to the z direction. The shape of the ex-

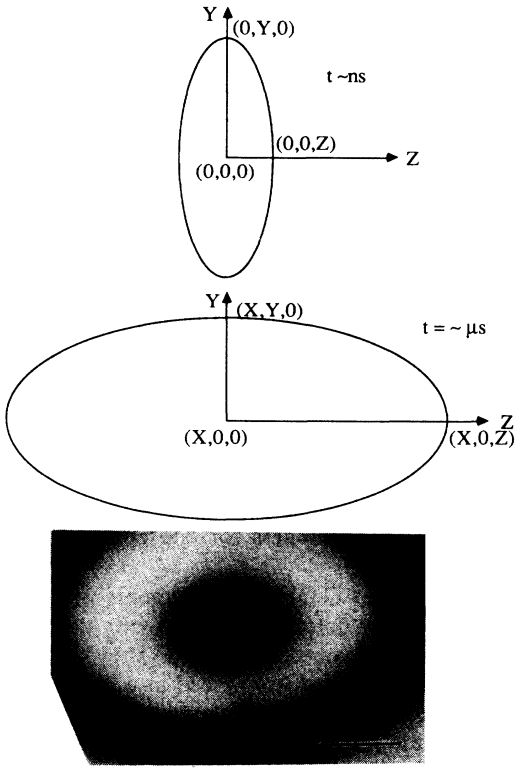

FIG. 3. (a) Schematic diagram showing the initial elliptical plasma shape after termination of the laser pulse, and (b) the final shape of the plasma before it strikes the substrate. The major axis of both of these diagrams are perpendicular to each other. (c) Actual shape of the deposit from a 1:2:3 target on Si showing equithickness contours.

panding plasma controls the density distribution of particles in it. Thus, elliptical isothickness contours similar to the plasma shape after expansion should be observed in the film. Figure 3(c) shows the shape of a 1:2:3 film deposited on silicon, which is in good agreement with the above prediction. The irradiated target spot was elliptical in shape in these experiments because of the angular incidence (45°) of the laser beam on the target.

III. RESULTS AND DISCUSSION

The differential equations controlling the expansion of the plasma have been solved numerically to understand the salient features of the laser-deposition process and were compared with the experimental results presented elsewhere.[11,15] The majority of the experimental data has been obtained for pulsed excimer-laser irradiation of multicomponent 1:2:3 targets for the formation of thin films. Experiments on multicomponent targets provide information on the effect of different atomic species on the nature of the deposition process. Equations (8) and (13) describe the three-dimensional expansion of the plasma in the isothermal and adiabatic regimes, respectively. These equations were numerically solved to simulate the expansion of the plasma as a function of time. The Runge-Kutta method with very small time steps was used to solve the differential equation in both expansion regimes. Since the expansion kinetics are dependent on the dimensions of the plasma, very small time steps were necessary to model the initial expansion process. In the isothermal regime, the time step was of the order of 0.01 psec in the first nanosecond of the expansion, whereas in the adiabatic regime, it was of the order of 100 psec. In the latter stages of the expansion, the time interval was increased by a factor of 10 or more without affecting the simulation results. Based on the above model, detailed simulations were carried out to understand the nature of and to obtain salient features in the PLE process. The salient features studied in detail were as follows: (i) dynamics of the laser deposition processes, (ii) spatial thickness variation, (iii) effect of energy density, (iv) effect of substrate-target distance and irradiated spot size, and (v) spatial compositional variations and the effect of atomic mass on plasma velocities. In each case the calculated values were compared with the available experimental results. All the calculations presented here have been carried out with assumed values of the plasma temperature T, specific heat capacity ratio γ, and the surface evaporation temperature.

A. Dynamics of laser-deposition process

The kinetics of the laser-deposition process can be obtained from a calculation of the time history of the plasma expansion velocities and dimensions which are shown in Figs. 4(a) and 4(b), respectively. These calculations were performed for XeCl ($\lambda=308$ excimer, $\tau=45$ nsec)

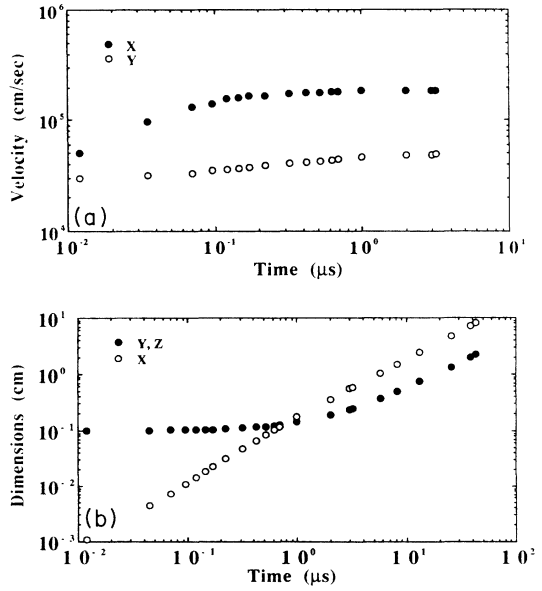

FIG. 4. Time history of transverse (y,z) and perpendicular (x) (a) velocities and (b) dimensions in the plasma formed by excimer-laser irradiation of 1:2:3 targets. A plasma temperature of 10 000 K, evaporation temperature of 2200 K, and an irradiated spot size of 2×2 mm were employed in the calculations.

laser irradiation of 1:2:3 bulk superconductor with an irradiated spot size of 2 mm×2 mm. An evaporation temperature of 2200 K, a plasma temperature of 10 000 K, an atomic weight of 89.0 (corresponding to the atomic weight of Y), and $\gamma = 1.66$ were employed in the calculations. The evaporation temperature, which controls the velocity of the particles leaving the surface, is close to experimental vaporization values for 1:2:3 bulk superconductors. Figure 4(a) shows the transverse (Y,Z) and perpendicular (X) velocity of the plasma edges during the initial stages of expansion. The dimensions of the edges in the perpendicular and the transverse directions are shown in Fig. 4(b). In the initial stages of plasma expansion, the velocity in the direction perpendicular to the surface is very high as a result of the small dimension of the plasma in that direction; the plasma edge reaches a maximum asymptotic velocity in about 1 μsec. The asymptotic velocity attained by the X edge is about 1.85×10^5 cm/sec, while for the Y edge, the asymptotic velocity corresponds to 4.95×10^4 cm/sec. It should be noted that in our theoretical model we have defined the plasma edge as the distance from the center where the density is 60.5% of the maximum value. Thus, for an exponentially decreasing density and linearly increasing velocity profile, higher velocities corresponding to 2–3 times X dimension are present, although the particle density is much lower at these distances. The acceleration in the transverse direction is not as high as that in the perpendicular direction because of the larger initial lateral dimensions of the plasma. Initially, the transverse velocities are about 3×10^4 cm/sec, which accelerate to an asymptotic velocity of 4.95×10^4 cm/sec after 1 μsec. These anisotropic expansion velocities give rise to changing plasma dimensions as shown in Fig. 4(b). After 0.7 μsec the lateral and the perpendicular dimensions of the plasma are equal (about 0.12 cm). As the X velocity is higher, the plasma preferentially elongates perpendicular to the surface, in agreement with the experimental results. It should be noted that the terminal velocity values have been obtained by assuming the ratio of heat capacities to be 1.66, which corresponds to monoatomic gases. However, if we account for the degrees of freedom associated with ionization and excitation, the value of γ would be lower, probably in the range of 1.2–1.3.[39]

The temperature of the plasma as a function of time is shown in Fig. 5 for simulation conditions similar to Fig. 3. Initially, the expansion is isothermal during the time interval of the laser pulse when the temperature remains constant. After the laser pulse terminates, the plasma expands adiabatically. The thermal energy of the plasma is converted into kinetic energy, and the plasma cools rapidly. Within 0.3 μsec of the laser pulse, the plasma cools from 10 000 K to about 2000 K. As seen from the adiabatic equation of state, the rate of temperature decrease is strongly dependent on the specific heat capacity ratio γ. The temperature may decrease much more slowly than predicted by the adiabatic equation due to recombination effects. When the thermal energy is of the order of 0.1 eV, the temperature starts to decrease less rapidly due to the energy released by the recombination of the ionized species in the plasma. the increase in energy due to these recombinations compensates for the cooling due to the expansion process.

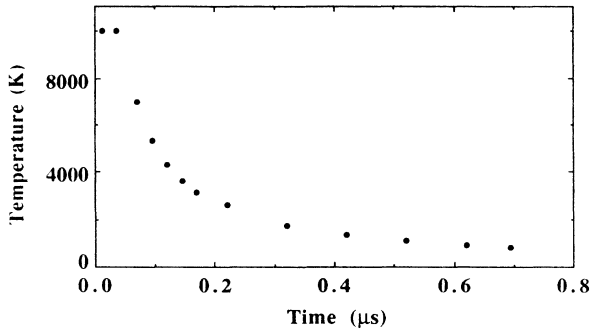

FIG. 5. The variation in plasma temperature as a function of time during plasma expansion under the same conditions as shown in Fig. 4.

The time-of-flight (TOF) measurements provide an excellent technique to determine the velocity distribution of the species in the plasma. Figure 6(a) shows typical TOF data obtained for a substrate placed at a distance of 3 cm away from the target. The intensity on the TOF trace denotes the number of particles arriving between time t and $t+dt$. The simulation conditions were the same as mentioned earlier. The intensity of the atomic flux shows a fast rise and a slow decay similar to the experimental results observed by Zheng *et al.*[11] for the laser-irradiated 1:2:3 targets. The simulated atomic velocity distributions

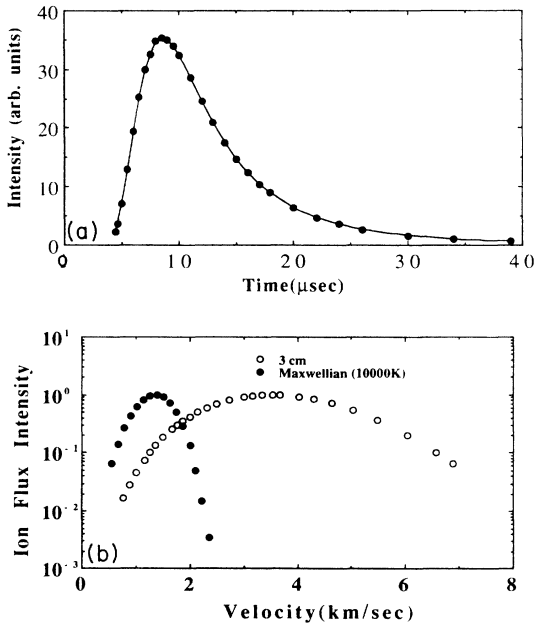

FIG. 6. (a) Simulated time-of-flight measurements and (b) atomic velocity distributions in the plasma formed by XeCl laser irradiation of 1:2:3 targets for Y atoms at an initial temperature of 10 000 K.

are plotted in Fig. 6(b) with the corresponding Maxwellian curve for a plasma temperature of 10 000 K. This figure clearly shows that the most probable velocity of ions in laser-generated plasma is about a factor of 3–4 higher than the Maxwellian most probable velocity, and the velocity distributions for the laser-evaporated species are much broader than expected from a thermal evaporation process. This broad velocity distribution has been experimentally verified by flux distributions obtained from laser-evaporated 1:2:3 targets.[11,12] In this case, the kinetic energy of the species is almost an order of magnitude greater than the thermal energies exhibiting the thermal nature of the laser-evaporated species. The kinetic energies corresponding to the plasma boundary are about 10–50 eV. Such energies are not typical of the particles present in the plasma since the velocity increases from zero at the center to maximum at the plasma edge and, furthermore, the plasma density is a monotonically decreasing function of distance from the target surface. Optical and ion time-of-flight measurements have shown that the most probable velocities for excimer-laser-irradiated 1:2:3 targets are of the order of 1.0×10^6 cm/sec, while in these theoretical calculations the most probable velocities are much lower. This can be explained by the effect of three factors. Firstly, in the calculations we have assumed a value of $\gamma=\frac{5}{3}$ which corresponds to the specific heat capacity ratios of unexcited monoatomic species. Because of the high plasma temperature, a high degree of excitation and ionization of the species is expected, which decreases the value of γ. It has been estimated[39] that the value of γ is in the range of 1.2–1.3 for excited monoatomic species, which has a strong effect on the terminal velocities as mentioned earlier. The second factor which affects the maximum velocity and the velocity distributions is the assumption that the exponentially varying density distribution is independent of γ. Detailed calculations have shown that[38] this assumption would lead to a $(\gamma-1)^{-0.5}$ dependence of the expansion velocity instead of the expected $(\gamma-1)^{-1.0}$ dependence. Thirdly, the maximum terminal velocities calculated by the formula $(v_{\max}=2a/\gamma-1)$ are valid only for one-dimensional isoentropic expansion. The dimensionality of the laser-generated plasma, although close to one, may deviate from this value depending on several factors including pulse energy density, plasma temperature, irradiated spot size, atomic mass of the species, etc.

Another intriguing experimental observation in the case of PLE generated species is the difference in both the velocity distribution and most probable velocity between the ionic and atomic species of the same element in the plasma.[40] The atomic species are characterized by lower most probable velocity and broader velocity distribution in comparison with the ionic velocities. Allen[41] has argued that transient electric fields in the plasma may not play an important part in the acceleration of the PLE species, and the above observations can be accounted for by the variation in the specific heat capacity ratio with the degree of ionization and the plasma temperature. Calculations are presently in progress to determine the effect of γ on the plasma dynamics.[38]

B. Spatial thickness variations

The thickness of the film at any point on the substrate, $\Delta x_f(y,z)$, can be determined by summing up all the particles (assuming a unity sticking coefficient) striking the substrate, and it is expressed as

$$\Delta x_f(y,z)\propto\int_0^{\alpha} n(x,y,z,t)\bar{v}(t)dt \ . \tag{14}$$

Figure 7 shows the simulated thickness variation of a film deposited on silicon. The simulation conditions were the same as mentioned in Fig. 4, where a plasma temperature of 10 000 K was assumed. This figure clearly shows that most of the evaporated material deposits preferentially in the region perpendicular to the irradiated target spot. The deposit is roughly Gaussian in shape with a full width at half maximum (FWHM) of approximately 15 mm. The curve also shows steep exponential variations in the thickness as the distance from the center of the deposit increases. The shape of the simulated curve closely matches the shape of the experimental curves obtained from excimer-laser irradiation of 1:2:3 targets.[15] The maximum thickness and FWHM of the deposit are dependent on the substrate-target distance, irradiated spot size, and energy density of the laser pulse.

C. Effect of pulse energy density

Pulse energy density is a very important parameter which controls both the thickness variation and composition of thin films. Experimentally, we have observed a more forward-directed deposition when the energy density is increased, and a simultaneous increase in the maximum thickness at the center of the deposit. To understand theoretically the effects of pulse energy density on the nature of laser deposition, we deduce its relation with the plasma temperature. From Eq. (13), we have observed that the acceleration and the expansion velocities

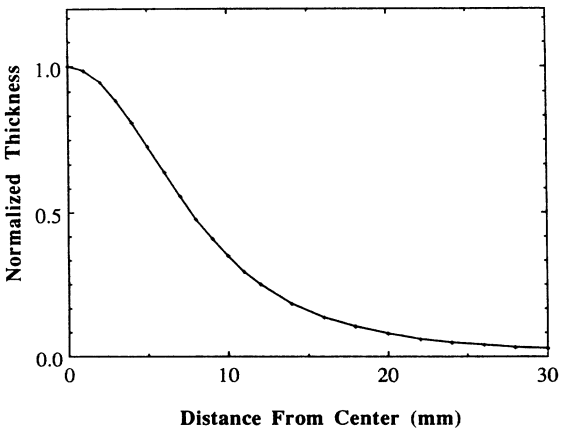

FIG. 7. Simulated curve showing spatial thickness variation as a function of distance from the center of the film deposited at a plasma temperature of 10 000 K and a substrate-target distance of 3 cm. An atomic weight of 89.0 was assumed in the calculations.

of the laser-generated plasma are dependent on initial isothermal temperature. From heat balance considerations, all the incident laser energy absorbed by the plasma per cm^2 per sec is converted into enthalpy E_h and kinetic energy E_k. At any given time, the power absorbed (P_{abs}) is related to the energy of the plasma by

$$P_{abs}=\frac{d}{dt}(E_k+E_h)\ . \tag{15}$$

The power absorbed by the expanding plasma at any time is given by

$$P[1-\exp(-\alpha_p x)]\ ,$$

where α_p is the average absorption coefficient of the plasma, and X is the dimension of the plasma in the direction perpendicular to the substrate. Here, P corresponds to the power density of the laser pulse which is proportional to the pulse energy density. If we assume that the energy absorbed by the plasma is small compared to the incident laser energy, the energy absorbed by the plasma can be simplified by expanding the exponential terms and neglecting the higher order terms. This results in the absorbed power given by ($P\alpha_p X$). Since the velocity and the concentration of the species in the plasmas are spatially varying, the total kinetic (E_k) and enthalpy (E_h) of the system are given by

$$E_k=\tfrac{1}{2}m\int_0^{\alpha} n(x,y,z)\bar{v}^2 dx\ , \tag{16}$$

$$E_h=h_2 m\int_0^{\alpha} n(x,y,z)dx\ , \tag{17}$$

where m is the mass of single atomic species and h_2 is the enthalpy per unit mass and is equal to $5kT/2m$ for a monoatomic gas. As T is proportional to v^2, the enthalpy per unit mass is also proportional to v^2. The integration of the above two equations shows that both the energy terms E_k and E_h are proportional to $(N_T\dot{X}^2 t/\tau)$. Thus Eq. (15) can be written as

$$P\alpha_p X\propto\frac{d}{dt}\left[\frac{N_T}{\tau}t\dot{X}^2\right]\ . \tag{18}$$

In an isothermal plasma formation and expansion regime, the velocity normal to the surface can be approximated to be independent of time when most of the laser energy is absorbed in the plasma. This has been verified from the dynamics of laser evaporation when maximum acceleration occurs within 1–2 nsec of the laser pulse. In the above expression, the velocity varies as the square root of the temperature ($T^{0.5}$), and the power density is proportional to the energy density divided by the pulse duration. However, the plasma absorption coefficient as seen from Eq. (3) depends on a variety of factors, including concentration of the ionized species, plasma temperature, and laser wavelength. The density of ionized species in turn is dependent on the evaporation rate, rate of plasma expansion, degree of ionization, etc. Dyer *et al.*[40] have observed that in the fluence range of 0.4–4.0 J/cm^2, a fractional ionization χ of 1.4%–4% for KrF laser-irradiated Y-Ba-Cu-O targets. It should also be mentioned that the temperature dependence of the absorption coefficient and the evaporation rate may not show a simple relationship with pulse energy density. The plasma expansion coefficient can be divided into two regimes depending on the ratio of the laser photon energy ($h\nu$) and the plasma thermal energy (kT). For $h\nu/kT\gg 1$, the absorption coefficient shows a $T^{-0.5}$ temperature and ν^3 frequency dependence, while in the reverse case ($h\nu/kT\ll 1$), the absorption coefficient shows a $T^{-1.5}$ and ν^2 frequency dependence. During PLE deposition of $YBa_2Cu_3O_7$ superconducting thin films when the plasma temperature is in the range of 1–2 eV, for excimer-laser irradiation the first regime is dominant, whereas for longer wavelength lasers (e.g., CO_2 laser, $\lambda=10.6\ \mu$m) the second regime is more applicable. For medium wavelength lasers, the temperature dependence is between $T^{-0.5}$ and $T^{-1.5}$, depending on the value of $h\nu/kT$. Some deviation from the above temperature dependence may occur if the free-free transitions involving ions are not the dominant absorption mechanism.

The degree of ionization of the evaporated species χ also depends on several factors, including plasma temperature, photon energy, etc. Higher plasma temperatures will lead to higher thermal ionization, whereas higher photon energy will give rise to higher photoionization. The shorter wavelength lasers have been found to be more efficient in generating higher ionized plasmas for Y-Ba-Cu-O targets,[37] thereby suggesting the role of photoionization and coupled photo and thermal excitations in the ionization process. Also, the variation of the degree of ionization with temperature (or pulse energy density) gives a mechanism for the ionization process. For a purely thermal ionization, the degree of ionization will show an exponential increase with temperature for partially ionized systems. However, of the KrF laser-irradiated 1:2:3 targets,[38] χ has been found to show a very weak dependence with energy density for $E>1.0$ J/cm^2, thus suggesting nonthermal mechanisms may be playing an important role in the ionization process. It should be noted that at energy densities near the vaporization threshold limit, other electronic mechanisms may also play an important part in the ionization process. For excimer-laser-irradiated 1:2:3 targets,[40] the degree of ionization has been found to be as high as 4% measured after the recombination and deexcitation effects have taken place. This tends to suggest that in the isothermal regime when the plasma has attained its maximum temperature, a much higher degree of ionization may be present. As the absorption cross section for ionized species is much larger than for neutral species, the bremsstrahlung process should be the primary absorption process as noted earlier. The mechanisms for absorption can change depending on the laser photon energy and the maximum temperature attained by the plasma.

Because of the different ionization mechanisms, the Saha equation cannot be explicitly used to determine the degree of ionization in these systems. The evaporation rate, as noted earlier, may also be not linearly dependent on energy density. If we assume that the ionization χ and particle density N_T are proportional to $(E-E_{th})^{\epsilon}$ and $(E-E_{th})^{\beta}$, respectively, the dependence of the absorption coefficient α_p on plasma temperature and pulse ener-

gy density can be written as

$$\alpha_p \propto \left[\frac{n_i^2}{T^\eta}\right] \propto \left[\frac{(E-E_{\rm th})^{2(\epsilon+\beta)}}{\tau^2 \dot{X}^2 T^\eta}\right], \quad (19)$$

where η corresponds to a value between 0.5 (low-temperature plasma) and 1.5 (high-temperature plasma). Substituting Eq. (19) in (18), the final expressions relating atomic velocity and plasma temperature with pulse energy density are given by

$$T \propto \left[\frac{E(E-E_{\rm th})^{2\epsilon+\beta}}{\tau^2}\right]^{2/(2\eta+3)}, \quad (20)$$

$$v \propto \left[\frac{E(E-E_{\rm th})^{2\epsilon+\beta}}{\tau^2}\right]^{1/(2\eta+3)}. \quad (21)$$

Thus, from the above equation it can be clearly seen that the dependence of the plasma temperature and expansion velocity on pulse energy density is controlled by the target evaporation rate and the degree of ionization. The above equations also predict that for the same temperature dependence of χ, the velocity of the longer wavelength laser-generated species will show a weaker dependence with energy density compared to shorter wavelength generated species. For excimer-laser-irradiated 1:2:3 targets, the value of η is equal to 0.5, β varies from 0.4 to 1.0, and ϵ varies from 0 to 0.5. Using the above values, the velocity is found to be proportional to E^δ, where δ is between 0.75 and 0.37. In this relation, δ decreases with an increase in energy density because of the change in the evaporation rate and the ionization conditions. In the case of excimer-laser-irradiated 1:2:3 targets, at high plasma temperatures (energy density greater than 2.0 J/cm^2), the ionization can be assumed to be independent of energy density. In this regime, the values of η, β, and ϵ can be approximated as 0.5, 0.5, and 0.0, respectively. If the pulse energy density is much higher than the threshold energy required for vaporization ($E \gg E_{\rm th}$), then Eq. (21) reduces to

$$v \propto E^{3/8}. \quad (22)$$

The exact value of the power exponent depends on the evaporation rate and the ionization efficiency as a function of energy density. The most probable atomic velocities of PLE species from KrF laser-irradiated 1:2:3 targets obtained from optical spectroscopy measurements by Zheng *et al.*[11] are reproduced in Fig. 8(a). At least-square fit curve is drawn for the experimental points. This experimental data show an $E^{0.3-0.4}$ dependence of atomic velocities with energy density. Other data published on the same system[41] show a similar agreement between pulse energy density and velocity, thus in agreement with the above model. Experiments are presently in progress to verify the above calculations.[38]

For longer wavelength laser-irradiated targets, the velocity dependence of the plasma species with energy density will be different. For a high-temperature plasma when most of the species are ionized, the velocity of PLE species will show a weaker dependence with energy density than compared to laser-irradiated targets. If we assume the same ionization and evaporation characteristics as in the excimer-laser-irradiated targets, the species velocities will show an E^δ dependence with energy density, the value of δ being between 0.5 and 0.23. For high plasma temperatures when the degree of ionization is independent of energy density, δ approaches the lower limit. Figure 8(a) shows the experimental data obtained by Sankur *et al.*[42] on the ionic velocities of different species after irradiation of ZrO_2 targets with a pulsed CO_2 laser ($\lambda = 10.6$ μm) at different energy densities. The ion velocity curves approximately a cube root dependence with energy density for both species. More *in situ* plasma dynamics are required to confirm the effect of the energy density and laser wavelength on the velocity of the PLE species.

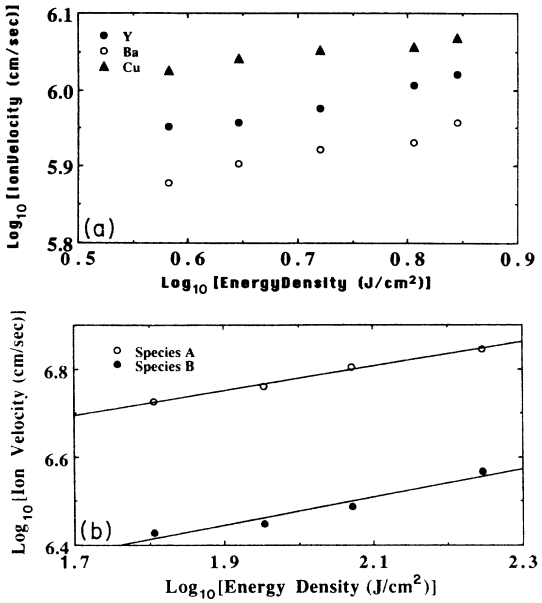

FIG. 8. Experimental atomic velocity data as a function of energy density for various species; (a) excimer-laser irradiated 1:2:3 target obtained from the data of Zheng *et al.* (Ref. 11). (b) CO_2 laser-irradiated ZrO_2 [obtained from the data of Sankur *et al.* (Ref. 42)].

Theoretically, the expansion characteristics are dependent on the plasma temperature and in turn on the energy density of the laser pulse. Pulse energy density affects both transverse as well as perpendicular expansion velocities of the plasma. Figure 9 shows the perpendicular and the transverse velocities as a function of plasma temperature for 1:2:3 targets. The perpendicular velocity of the X edge shows a square root dependence with plasma temperature, but the temperature dependence of the transverse velocity is much weaker. As we increase the plasma temperature, the perpendicular velocity increases much faster in comparison to the transverse velocity. This gives rise to a more forward-directed nature of the deposited material, in agreement with the experimental results presented elsewhere.[15]

The simulated spatial thickness variations for plasma temperatures of 4000, 8000, and 12 000 K are shown in

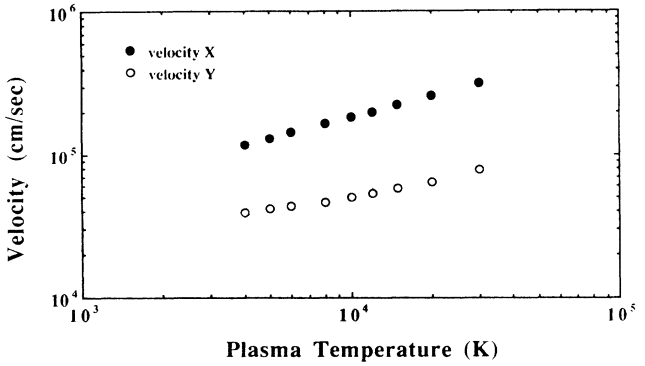

FIG. 9. Transverse and perpendicular velocities of Y species in the plasma as a function of the plasma temperature for excimer-laser-irradiated 1:2:3 targets.

TABLE I. The effect of plasma temperatures on maximum thickness due to anisotropic plasma expansion, full width at half maximum of the deposit, and the ratio of the maximum thickness with thickness at 15 mm (t_{15}) and 25 mm (t_{25}) away from the center. An atomic weight of 89 and a substrate target distance of 3 cm was employed in the calculations.

Temperature (K)	t_{max}	FWHM	t_{max}/t_{15} (mm)	t_{max}/t_{25}
4000	0.564	18.80	4.11	13.35
5000	0.640	17.71	4.64	15.50
6000	0.700	17.00	5.10	17.76
8000	0.789	16.00	5.78	20.86
10000	0.855	15.40	6.34	23.30
12000	0.899	15.00	6.68	25.00
15000	0.951	14.64	7.13	27.11
20000	1.000	14.20	7.56	29.00
30000	1.033	14.00	7.87	30.21

Fig. 10(a). The simulation parameters are the same as mentioned in Fig. 4. The maximum thickness, which is at the center of the deposit, increases with increasing plasma temperature. The maximum spatial thickness variations, which occur roughly at a distance of 4–8 nm away from the center of the deposit, also increase with the plasma temperature. At larger distances from the center (> 12 mm), the thickness of the deposit formed at lower plasma temperatures is slightly higher. This is due to the fact that the total number of evaporated particles in the simulation experiments remains constant. Table I provides details of the energy variation of the FWHM, and the ratio of the thickness of the deposit at 15 mm and 25 mm away from the central spot. The table shows that the FWHM of the deposit decreases with an increase in energy density of the laser pulse, with a corresponding increase in the spatial thickness variations.

Figure 10(b) shows the maximum thickness of the deposit as a function of energy density. In these calculations, we have assumed that a fixed number of particles are evaporated at all plasma temperatures. The variation in the maximum thickness shown in this figure is only due to the anisotropic expansion characteristics of the plasma. The graph shows that with an increase in the plasma temperature (pulse energy density), there is a nonlinear increase in the maximum thickness of the deposit. For low energy densities, the maximum thickness increases very rapidly. The perpendicular velocities are

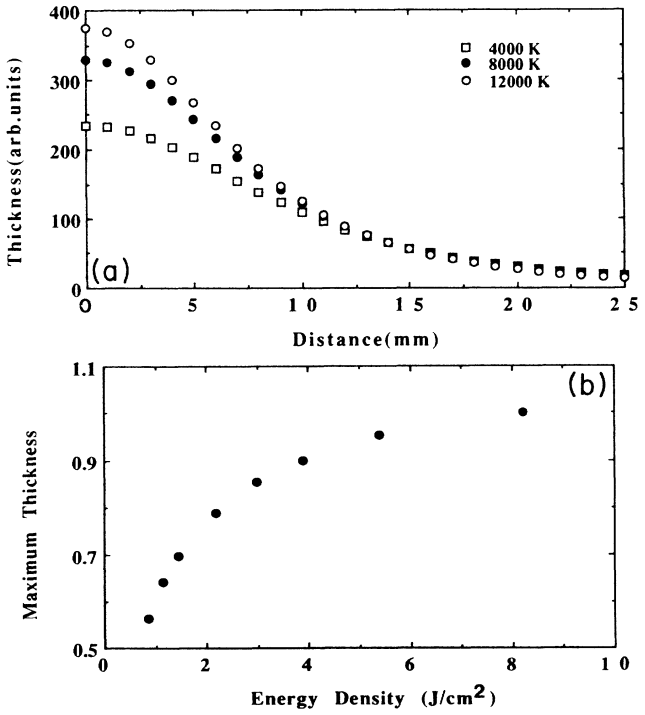

FIG. 10. (a) Simulated thickness variations as a function of distance from the center of the film, for plasma temperatures corresponding to 4000, 8000, and 15000 K, respectively. (b) The variation in the maximum thickness (at the center of the film) as a function of energy density assuming the same evaporation flux and irradiated spot size.

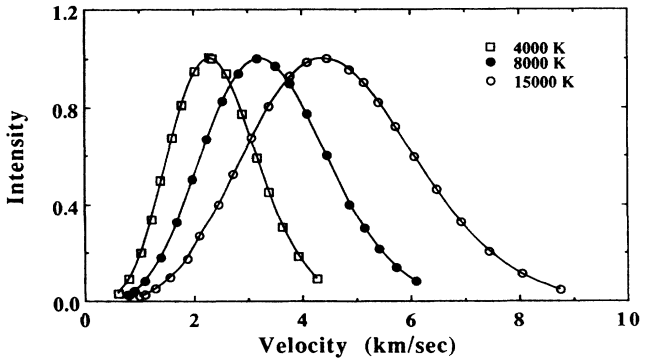

FIG. 11. The intensity distribution for Y atomic velocities in a plasma generated by excimer-laser irradiation of 1:2:3 targets for plasma temperatures of 4000, 8000, and 15000 K.

more sensitive to the plasma temperature than compared to the transverse velocities. With an increase in plasma temperature, the perpendicular velocities change more rapidly, resulting in the steep maximum thickness variations.

Figure 11 shows atomic velocity distributions corresponding to plasma temperatures of 4000, 8000, and 15 000 K. The above calculation simulates velocity distributions of Y atoms (atomic weight 89.0) generated during excimer-laser irradiation of 1:2:3 targets. The shape and the velocity distribution of the curves are non-Maxwellian in nature. The velocity distribution can be modeled as a simple Maxwellian distribution superimposed on a drift velocity term. From the results, we can derive a square-root dependence with temperature of the most probable velocity of atomic species and the FWHM of the velocity distribution.

D. Effect of substrate-target distance and irradiated spot size

In this subsection, we analyze the effect of the substrate parameters, including the substrate-target distance and irradiated spot size. (See Table II.) Figure 12(a) shows the spatial thickness variation of the deposit for a substrate-target distance of 3 cm, 5 cm, and 7 cm, respectively. The maximum thickness at the center of the deposit decreases appreciably with the increase in substrate-target distance, while the FWHM of the deposit increases. The variation in the maximum thickness of the deposit with substrate-target distance d can be expressed in the form of d^{-p}, where p is the expansion coefficient describing the nature of the expansion. The value of p corresponds to 3 for a three-dimensional spherical expansion and is equal to 1 for a linear expansion in one dimension. We have found that this expansion coefficient is dependent on the spot size. The expansion coefficient is plotted as a function of the laser-irradiated spot size in Fig. 12(b). This graph shows that for larger spot sizes, the expansion of the plasma tends towards the one-dimensional value. As the spot size is decreased, the expansion becomes more spherical. This observation can be explained by Eq. (13), which shows that the acceleration is inversely proportional to the irradiated spot size. In these calculations, the same parameters were adopted as in Fig. 4.

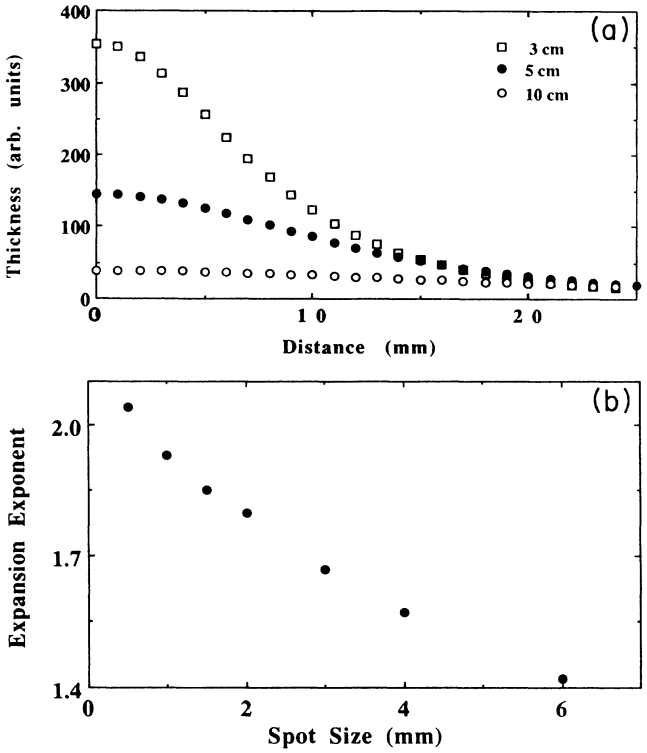

FIG. 12. (a) The spatial thickness variation in a PLE film deposited at substrate-target distances of 3, 5, and 7 cm and (b) the variation in the power expansion coefficient as a function of irradiated spot size. A plasma temperature of 10 000 K was employed in the calculations.

TABLE II. The effect of the substrate-target distance on the normalized maximum thickness (t_{max}), full width at half maximum (FWHM), ratio of thicknesses at 28 (t_{28}) and 48 (t_{48}) mm from the center with the maximum thickness of the deposit. An atomic mass of 89, plasma temperature of 10 000.0, and an irradiated spot size of 2 mm×2 mm were employed in the simulations.

Substrate-target distance (cm)	t_{max}	FWHM (mm)	t_{max}/t_{28}	t_{max}/t_{48}
2	1.97	7.31	96.6	477.3
3	1.0	15.8	35.3	165.2
5	0.41	23.6	10.5	43.4
7	0.22	31.8	5.3	18.7
10	0.11	43.9	2.88	8.1
15	0.05	62.5	1.79	3.7

E. Spatial compositional variations

We have shown in Eq. (13) that the velocity and the acceleration of the species depend on the atomic mass. According to this equation, the asymptotic velocity of the ionic species should be inversely proportional to the square root of its molecular weight. This dependence should be followed in cases where the species are noninteracting, for example, in comparison of velocities of species from single component targets. In the case of multicomponent targets, the measured experimental velocities show a general trend of lower asymptotic velocities for higher masses; however, the observed dependence is much weaker than expected. In the case of laser-ablated 1:2:3 targets,[11] the ratio of the velocities of Cu to Ba was found to be 1.36, whereas the ratio of the inverse square root of their masses is approximately 1.6. Similar dependence has been observed in the case of pulsed CO_2 laser-ablated ZrO_2 targets,[42] where the ratio of the light-

est and heaviest cation is 1.35, compared to the ratio of the inverse square root of their masses, which is 2.76. This discrepancy is probably due to the interaction of different atomic species in the plasma. At any fixed temperature, the velocity of the lighter species will be greater than the velocity of the heavier species. But during the initial stages of expansion, when the particle density is of the order of $10^{19}-10^{20}$ cm^3, a continuum model applies and all the species must expand together with a uniform average velocity. After the initial stages of expansion, when the plasma density drops, all the individual particles are initially accelerated to an asymptotic velocity. Thus, the dependence of ion velocities is less than the predicted inverse square root dependence.

Based on the experimental observations, we have simulated the XeCl laser irradiation on multielement 1:2:3 targets. Figure 13 shows the velocity of different species as a function of atomic weight. In these calculations, a plasma temperature of 10 000 K and an average molecular weight of 89.0 was assumed during the isothermal regime, but in the adiabatic regime, it was dependent on their respective atomic weights. Due to a large number of collisions taking place in the initial stages of isothermal expansion of the plasma, an average atomic weight was used to calculate its expansion characteristics. The velocity of the atomic species shows a weaker dependence with atomic weight than expected from a noninteracting process. In the case of laser-irradiated 1:2:3 superconductors, we have calculated the velocity variations as $M^{-0.37}$, where M is the atomic mass of the species. Table III shows variations with atomic weight for perpendicular expansion velocities, for interacting and noninteracting plasmas, and the composition variations at the thickest spot formed at the center of the deposit. This table shows that the atomic velocities in the interacting plasma exhibit a much weaker dependence on the atomic mass compared to atomic velocities in a noninteracting plasma. The atomic mass dependence of the perpendicular velocity (X) results in spatial compositional variations in thin films. The experimentally obtained compositional variations for multielemental Y-Ba-Cu-O targets,[15] and the atomic velocities of species in

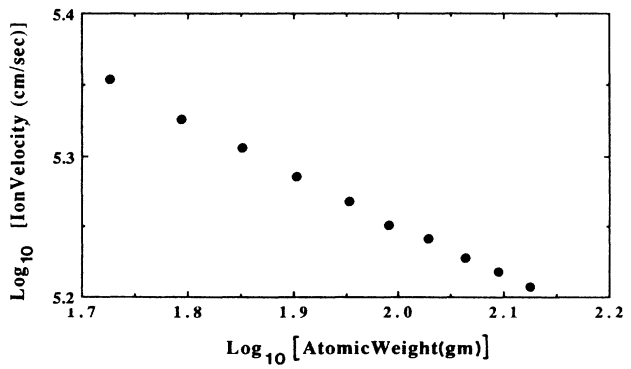

FIG. 13. Velocity of different ionic species as a function of atomic weight in an interacting plasma. A plasma temperature of 10 000 K was employed in the calculations.

TABLE III. This table shows the ratio of perpendicular and transverse velocities (v_{ratio}), the maximum thickness ($t_{\max}$) at the center of the deposit, and the perpendicular velocities normalized with velocity corresponding to atomic weight of 53 g (v/v_{53}) for different atomic weights (AW) species present in an interacting plasma. This value is compared with the inverse square root of the atomic mass relationship. A substrate-target distance of 3 cm and a plasma temperature of 10 000 K was employed in the calculations.

Atomic weight	v_{ratio}	$t_{\max}$	v_{AW}/v_{53}	$(m_{53}/m_{\text{AW}})^{1/2}$
53	3.91	1.0	1.0	1.0
71	3.81	0.94	0.893	0.862
89	3.73	0.90	0.819	0.769
107	3.66	0.87	0.770	0.709
125	3.60	0.85	0.730	0.653

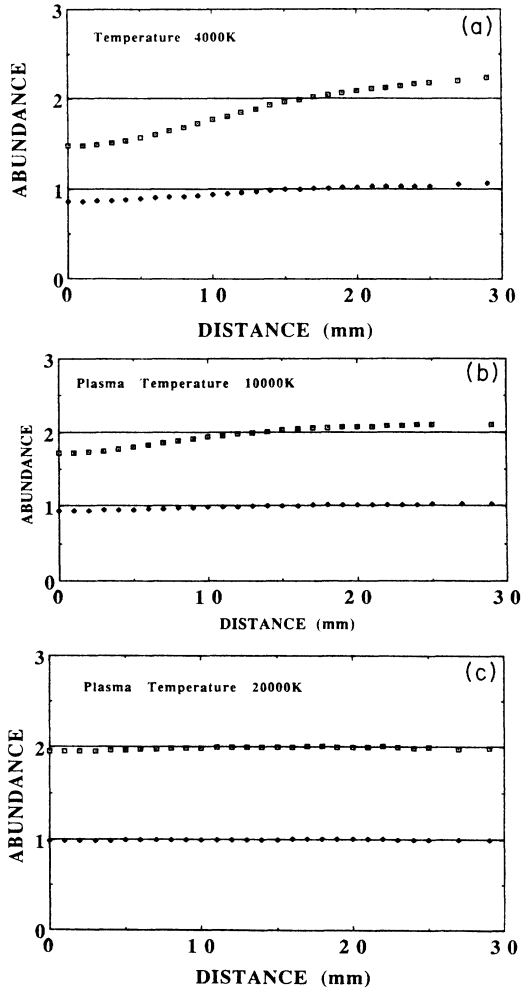

FIG. 14. Spatial compositional deviations from stoichiometric values of Y, Ba, and Cu in interacting plasmas for plasma temperatures of (a) 4000 K, (b) 8000 K, and (c) 15 000 K. A stoichiometric evaporation of the 1:2:3 target was assumed.

TABLE IV. The variation in the simulated spatial composition of an excimer-laser-evaporated stoichiometric 1:2:3 film for different plasma temperatures at a substrate-target distance of 3 cm. The compositional values for Y and Ba of film at 0, 15, 25, and 33 mm away from the center are shown. These values have been normalized with copper, which is equal to 3.0.

Temperature (K)	0 mm		15 mm		25 mm		33 mm	
	Y	Ba	Y	Ba	Y	Ba	Y	Ba
4000	0.87	1.48	0.99	1.96	1.05	2.18	1.07	2.26
6000	0.89	1.57	1.00	2.01	1.04	2.16	1.05	2.22
10000	0.93	1.72	1.00	2.03	1.03	2.12	1.04	2.12
20000	0.99	1.96	1.00	2.00	1.00	2.00	1.01	2.03

the plasma were compared with the simulation results for laser-irradiated 1:2:3 targets.[11] These calculations were performed assuming that collisions would lead to an average expansion velocity in the isothermal regime.

We have observed experimentally that stoichiometric evaporation from bulk 1:2:3 targets occurs at energy densities greater than 1.5 J/cm^2. However, spatial compositional variations can occur in the film even when the evaporation is stoichiometric. Figures 14(a), 14(b), and 14(c) show the spatial compositional variations for plasma temperatures of 4000 K, 10 000 K, and 20 000 K, respectively. These calculations were performed for stoichiometric evaporation from the target, i.e., the target material is evaporated with 1:2:3 ratio for Y-Ba-Cu. The ratios of the Y and Ba values are normalized to Cu, whose value is kept constant at 3.0. The stoichiometric values of Y and Ba are shown by horizontal lines in the figure. The results show that at low energy densities, the composition of the lightest species (Cu) is larger than its stoichiometric value near the center of the deposit, and decreases as the distance from the center of the deposit increases. As the energy density (plasma temperature) increases, the spatial compositional variations decrease, converging to 1:2:3 stoichiometric value. These curves also show that the ratio of each species is spatially different. For example, at a plasma temperature of 4000 K, the ratio of [Cu]/[Ba] is 2.03, 1.38, and 1.33 at distances of 0 mm, 25 mm, and 33 mm from the center of the film, respectively. Table IV lists the composition variation at different points in the film for various plasma temperatures (energy density). This table shows that for a fixed energy density, compositional variations are present both at the center of the deposit and at large distances away from the center. At a distance of about 7–10 mm away from the center, the deposition is stoichiometric, in agreement with the experimental results.[15] The compositional variations increase with increasing distance from the center of the deposit. The shape and the trend of the composition variation curves at different energy densities are in agreement with the experimental results presented elsewhere.[15]

These compositional variations in multielemental films are attributed to the different atomic velocities of the species in the plasma. The particle velocities show a weaker than inverse square root dependence with the molecular weight, as explained earlier. Table V shows a comparison of the ratios of the atomic velocities at different plasma temperatures with the experimental values obtained by Zheng *et al.*[11] From excimer-laser irradiation of 1:2:3 targets, the ratio of the velocities of Cu to Ba, and Cu to Y was found to be 1.33 and 1.16, respectively. These ratios were almost independent of energy

TABLE V. Comparison of the experimental and simulated velocities of atomic species in laser-irradiated 1:2:3 targets. The experimental values were obtained from the data of Zheng *et al.* (Ref. 11). The velocity values have been normalized to the velocity of copper.

Temperature (K)	Energy density (J/cm^2)	Simulated		Experimental	
		v_{Cu}/v_Y	v_{Cu}/v_{Ba}	v_{Cu}/v_Y	v_{Cu}/v_{Ba}
4000		1.16	1.33		
6000		1.15	1.35		
	2.55			1.19	1.38
10000		1.14	1.33		
	3.80			1.18	1.40
	5.25			1.19	1.35
	6.4			1.12	1.33
	7.0			1.12	1.30
20000		1.14	1.33		

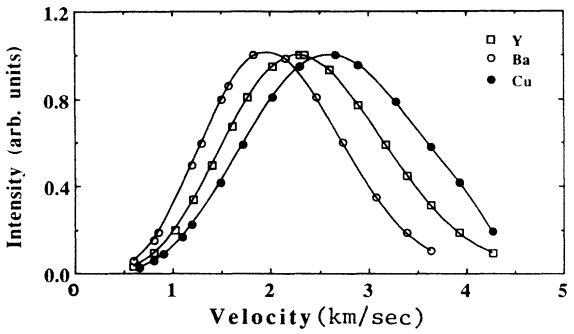

FIG. 15. The intensity of Cu, Y, and Ba atoms as a function of the velocity in plasmas generated by excimer-laser irradiation of 1:2:3 targets. A plasma temperature of 4000 K was assumed.

density. The above values are in good agreement with the experimental results, thus confirming the validity of the model

Figure 15 shows the simulated velocity distributions of Y, Ba, and Cu atomic species generated by excimer-laser irradiation of 1:2:3 targets. A plasma temperature of 10 000 K corresponding to an energy density of 3.0 J/cm^2 was employed in the calculations. The figure shows that the most probable velocity of the species in the plasma increases with a decrease in the atomic weight. The increase is weaker than the inverse square root dependence of the atomic mass as a result of the interactive nature of the plasma. Also, the FWHM of the velocity distribution shows a similar dependence on the atomic weight of the species.

IV. SUMMARY AND CONCLUSIONS

The details of the physical phenomena involving the interaction of nanosecond laser pulses with single-element and multielement targets, resulting in evaporation, plasma formation, and subsequent deposition of thin films, is considered. A theoretical model simulating these effects and interaction processes has been proposed. At high power densities obtained from nanosecond excimer-laser pulses, heating and evaporation of the material will occur at the beginning of the laser pulse. The amount of evaporated flux varies linearly with the pulse energy density. As the evaporated material is further heated by the interaction of the laser beam, it results in the formation of a high-temperature plasma of ions, atoms, molecules, electrons, etc. The temperature attained by the plasma depends on the power density, frequency, pulse duration of the laser beam, and the optical and thermophysical properties of the material. This plasma can be simulated as a HP-HT gas which is initially confined to small dimensions, and then is allowed to expand in vacuum. The plasma is treated as a compressible fluid, and the gas dynamics equations are set up to simulate its expansion. During the incidence of the laser pulse, the isothermal expanding plasma is constantly augmented at its inner surface with evaporated particles from the target. The plasma is assumed to have exponential density gradients, and the velocity of various species varies linearly from the center of the plasma. The acceleration and the expansion velocities in this regime are found to depend upon the initial velocities of the plasma. Because of the large lateral dimensions of the plasma, it expands preferentially normal to the irradiated surface. After the termination of the laser pulse, this plasma expands adiabatically with the expansion velocities controlled by its initial dimensions. The plasma cools rapidly during the expansion process, with the edge velocities reaching asymptotic values. The particles from the expanding plasma strike the substrate and form a thin film with characteristic spatial thickness and composition variations.

The solutions of the gas-dynamic equations show that the expansion velocities are related to the initial dimensions and temperature of the plasma, and the atomic weights of the respective species. Detailed calculations from the model have been presented. Because of the large lateral dimensions of the focused laser spot, the plasma expands preferentially normal to the target surface. The forward-directed nature of the plasma deposition was found to be a direct result of the anisotropic expansion velocities of the plume, which are derived by the density gradients in the plasma. The simulated spatial thickness curves were found to closely match the experimental data for laser-irradiated 1:2:3 superconductors. Velocity distributions of laser-evaporated species exhibited much higher kinetic energies than expected from a Maxwellian thermal distribution. The energy density was found to control the plasma temperature, which dictated the anisotropic expansion velocities of the plasma. From energy balance considerations, the dependences of plasma temperature and expansion velocities were determined as a function of pulse energy density. The non-Maxwellian nature of the velocity distributions was analyzed as a function of plasma temperature. Higher energy densities were found to result in higher plasma temperatures and a more forward-directed deposit. Other factors that affect the thickness variations are the irradiated spot size and the substrate-target distance. Larger substrate-target distances and spot sizes increased the uniformity of the deposit and reduced the spatial thickness variation in the film.

Though the expansion equation predicted an inverse square-root dependence of the atomic velocities with the respective masses, the dependence was found to be much weaker for laser-irradiated multielemental targets. A weaker dependence was attributed to the collisions occurring in the plasma during the initial stages of the expansion process. The calculations for laser irradiation of multielement targets were accomplished by using an average velocity during the initial stages of isothermal expansion when the mass free path of the particles is very small. These calculations were performed for spatial compositional variations in stoichiometrically evaporated 1:2:3 targets for various plasma temperatures. The calculations showed that a higher concentration of lower atomic mass species was deposited at the center of the deposit, in agreement with the experimental results. At large distances away from the center, the concentrations of the heavier atomic weight species were larger than the

stoichiometric values. For higher energy densities, spatial variations in composition decreased as the compositions converged to the stoichiometric value. The calculations were also able to predict and show the dependence of atomic velocities on atomic mass of different species in the plasma. The calculated results were in agreement with the experimental results. Thus, the model presented in this paper is found to explain salient features observed in the laser-deposition process. However, it must be noted that all the calculations are based on the assumed values of the plasma temperature, specific heat capacity ratio, etc. Thus, the experimental determination of the plasma absorption coefficient on various factors is extremely important in estimating the effect of laser parameters (energy density, wavelength, pulse duration, etc.) and material parameters on the deposition process.

ACKNOWLEDGMENTS

Part of this research was sponsored by the office of Energy Systems Research, Division of Energy Conversion and Utilization Technologies (ECUT) programs under Subcontract No. 19X-4337C, the U.S. Department of Energy, Martin Marietta Energy Systems, Inc., Oak Ridge National Laboratories, and National Science Foundation under Project No. 8618735. The authors would like to thank Deepika Bhattacharya for help in the computer simulation work.

[1]D. Dijjkamp, T. Venkatesan, X. D. Wu, S. A. Shaheen, N. Jisrawi, Y. H. Min-lee, W. L. McLean, and M. Croft, Appl. Phys. Lett. **51**, 619 (1987).

[2]J. Narayan, N. Biunno, R. Singh, O. W. Holland, and O. Auchiello, Appl. Phys. Lett. **51**, 1845 (1987).

[3]A. M. Desantolo, M. L. Mandich, S. Sunshine, B. A. Davidson, R. M. Fleming, P. Marsh, and T. Y. Kometani, Appl. Phys. Lett. **52**, 1995 (1988).

[4]K. Moorjani, J. Bohandy, F. J. Adrian, B. F. Kim, R. D. Shull, C. K. Chiang, L. J. Swartzebdruber, and L. H. Benett, Phys. Rev. B **36**, 4036 (1988).

[5]N. Biunno, J. Narayan, S. Hofmiester, A. K. Srivatsa, and R. K. Singh, Appl. Phys. Lett. **54**, 1519 (1989).

[6]H. S. Kwok, J. P. Zheng, S. Witanachchi, P. Mattocks, L. Shi, Q. Y. Ying, X. W. Wang, and D. T. Shaw, Appl. Phys. Lett. **52**, 1095 (1988).

[7]D. K. Fork, J. B. Boyce, F. A. Ponce, R. I. Johnson, G. B. Anderson, G. A. N. Connell, C. B. Eom, and T. H. Geballe, Appl. Phys. Lett. **53**, 337 (1988).

[8]C. Richard Guarieri, R. A. Roy, K. L. Saenger, S. A. Shivshankar, D. S. Yee, and J. J. Cuomo, Appl. Phys. Lett. **53**, 532 (1988).

[9]W. A. Weiner, Appl. Phys. Lett. **52**, 2171 (1988).

[10]R. K. Singh, O. W. Holland, and J. Narayan, J. Appl. Phys. (to be published).

[11]J. P. Zheng, Z. Q. Huang, D. T. Shaw, and H. S. Kowk, Appl. Phys. Lett. **54**, 280 (1989).

[12]T. Venkatesan, X. D. Wu, A. Inam, Y. Jeon, M. Croft, E. W. Chase, C. C. Chang, J. B. Watchman, R. W. Odom, F. Radicati di Brozolo, and C. A. Magee, Appl. Phys. Lett. **53**, 1431 (1988).

[13]T. Nakayama, M. Okigawa, and N. Itoh, Nucl. Instrum. Methods **B1**, 301 (1984).

[14]B. J. Stritzker *et al.*, Phys. Rev. Lett. **47**, 356 (1982).

[15]R. K. Singh and J. Narayan (unpublished).

[16]R. K. Singh, N. Biunno, and J. Narayan, Appl. Phys. Lett. **53**, 1013 (1988).

[17]R. A. Neifeld, S. Gunapala, C. Liang, S. A. Shaheen, M. Croft, J. Price, D. Simons, and W. T. Hill III, Appl. Phys. Lett. **53**, 703 (1988).

[18]T. Venkatesan, X. D. Wu, A. Inam, and J. B. Watchman, Appl. Phys. Lett. **52**, 1193 (1987).

[19]R. F. Wood and G. E. Giles, Phys. Rev. B **23**, 2923 (1981).

[20]R. K. Singh and J. Narayan, Mater. Sci. Eng. B **3**, 217 (1989).

[21]A. Inam, X. D. Wu, T. Venkatesan, S. B. Ogale, C. C. Chang, and D. Dijjkamp, Appl. Phys. Lett. **51**, 1112 (1987).

[22]R. Kelly and E. Rothenberg, Nucl. Instrum. Methods B **7/8**, 755 (1985).

[23]D. B. Geohegan, D. N. Mashburn, R. J. Cubertson, S. J. Pennycook, J. D. Budhai, R. E. Valiga, B. C. Sales, D. H. Lowdnes, L. A. Boatner, E. Sonder, D. Eres, D. K. Christen, and W. H. Christie, J. Mater. Res. **3**, 1169 (1988).

[24]J. F. Ready, *Effects of High Power Laser Radiation* (Academic, New York, 1971).

[25]J. M. Dawson, Phys. Fluids **7**, 981 (1964).

[26]N. R. Isenor, J. Appl. Phys. **36**, 316 (1965).

[27]J. Dawson, P. Kaw, and B. Green, Phys. Fluids **12**, 875 (1969).

[28]A. F. Haught and D. H. Polk, Phys. Fluids **9**, 2047 (1966).

[29]A. Caruso and R. Gratton, Plasma Phys. **10**, 867 (1968).

[30]N. G. Basov, V. A. Boiko, V. A. Dement'ev, O. N. Krokhin, and G. V. Skilikov, Zh. Eksp. Teor. Fiz. **51**, 986 (1966) [Sov. Phys.—JETP **24**, 659 (1967)].

[31]W. L. Fader, Phys. Fluids **11**, 2200 (1968).

[32]A. W. Ehler, J. Appl. Phys. **37**, 4962 (1966).

[33]N. G. Basov and O. N. Krokhin, Zh. Eksp. Teor. Fiz. **46**, 171 (1964) [Sov. Phys.—JETP **19**, 123 (1964)].

[34]S. I. Andreev, Y. I. Dymshits, L. N. Kaporski, and G. S. Mustova, Zh. Tekh. Fiz. **38**, 875 (1968) [Sov. Phys.—Tech. Phys. **13**, 657 (1968)].

[35]H. Opower and E. Burfinger, Phys. Lett. **16**, 37 (1965).

[36]T. P. Hughes, *Plasma and Laser Light* (Wiley, New York, 1975).

[37]Q. Y. Ying, D. T. Shaw, and H. S. Kwok, Appl. Phys. Lett. **53**, 1762 (1988).

[38]R. K. Singh, R. Neifeld, and J. Narayan, J. Appl. Phys. (to be published).

[39]Zel'dovich and Raizer, *Physics of Shock Waves and High Temperature Phenomena* (Academic, New York, 1966).

[40]P. E. Dyer, R. D. Greenough, A. Issa, and P. H. Key, Appl. Phys. Lett. **53**, 534 (1988).

[41]F. J. Allen, J. Appl. Phys. **43**, 2175 (1972).

[42]H. Sankur, J. Denatale, W. Gunning, and J. G. Nelson, J. Vac. Sci. Technol. **A5**, 2869 (1987).

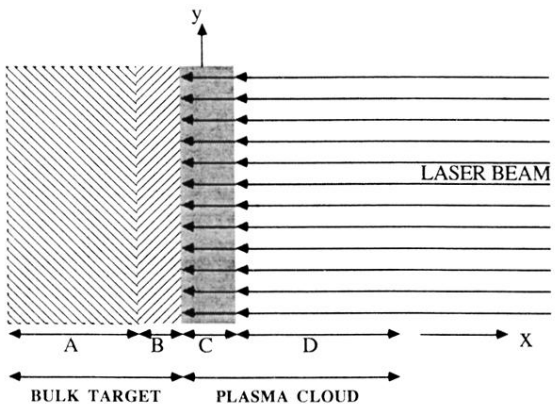

FIG. 1. Schematic diagram showing the different phases present during laser irradiation of a target: (*A*) unaffected target, (*B*) evaporated target material, (*C*) dense plasma absorbing laser radiation, and (*D*) expanding plasma outer edge transparent to the laser beam.

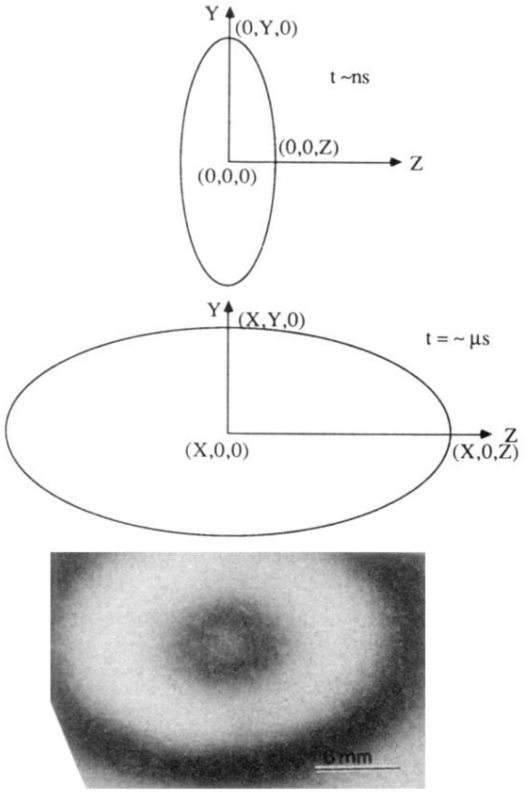

FIG. 3. (a) Schematic diagram showing the initial elliptical plasma shape after termination of the laser pulse, and (b) the final shape of the plasma before it strikes the substrate. The major axis of both of these diagrams are perpendicular to each other. (c) Actual shape of the deposit from a 1:2:3 target on Si showing equithickness contours.